Many-body localization and delocalization dynamics in the thermodynamic limit

Jonas Richter ●[*] and Arijeet Pal

Department of Physics and Astronomy, University College London, Gower Street, London WC1E 6BT, United Kingdom

Disordered quantum systems undergoing a many-body localization (MBL) transition fail to reach thermal equilibrium under their own dynamics. Distinguishing between asymptotically localized or delocalized dynamics based on numerical results is, however, nontrivial due to finite-size effects. Numerical linked cluster expansions (NLCE) provide a means to tackle quantum systems directly in the thermodynamic limit but are challenging for models without translational invariance. Here we demonstrate that NLCE provides a powerful tool to explore MBL by simulating quench dynamics in disordered spin-1/2 two-leg ladders and Fermi-Hubbard chains. Combining NLCE with an efficient real-time evolution of pure states, we obtain converged results for the decay of the imbalance on long time scales and show that, especially for intermediate disorder below the putative MBL transition, NLCE outperforms direct simulations of finite systems with open or periodic boundaries. Furthermore, while spin is delocalized even in strongly disordered Hubbard chains with frozen charge, we unveil that an additional tilted potential leads to a drastic slowdown of the spin imbalance and nonergodic behavior on accessible times. Our work sheds light on MBL in systems beyond the well-studied disordered Heisenberg chain and emphasizes the usefulness of NLCE for this purpose.

Introduction.– Many-body localization (MBL) extends Anderson localization to interacting quantum systems [1,2]. Based on seminal early works [3,4] and numerous subsequent studies (see e.g., Refs. [5–11]), it is believed that a disordered one-dimensional (1D) system with local interactions can undergo a transition from a thermal phase to a MBL phase for sufficiently strong disorder. The MBL phase is characterized, e.g., by a breakdown of the eigenstate thermalization hypothesis [12], area-law entangled energy eigenstates [13], and a logarithmic growth of entanglement in time [14,15]. Its properties can be understood in terms of an emergent set of local integrals of motion [16–19], so-called l-bits. Due to a finite overlap with these l-bits, observables fail to thermalize under time evolution, which makes MBL systems candidates for realizing quantum memories. This memory of initial conditions is a key experimental signature of MBL [20–22] but is theoretically investigated as well [23–25].

The emergent l-bit phenomenology of MBL motivated by nearest-neighbor qubit models can become unstable in higher dimensions [21,26–28] in the presence of non-Abelian symmetries [29–32], long-range interactions [33–36], large local Hilbert-space dimensions [37–39], and disorder-free systems [40–49]. Despite these instabilities of the fully MBL systems, they can show anomalously slow dynamics and even nonergodic behavior for certain initial conditions [50], referred to as the MBL *regime* [51]. For instance, in 2D signatures of the MBL regime exist in experiments and numerics [21,26–28], although in the thermodynamic limit the avalanche picture [52,53] suggests fully chaotic dynamics, albeit at astronomically long time scales.

The main complication for numerical studies of MBL is the presence of strong finite-size effects [51,54–59]. In this context, the existence of a genuine MBL phase (even for nearest-neighbor 1D models) has been put into question [60–62]. Providing a definite answer to this issue by means of numerical approaches is challenging. On one hand, full or sparse-matrix diagonalization methods are restricted to intermediate system sizes, potentially leading to inconclusive results. On the other hand, tensor-network techniques can treat large systems, but the times reachable in simulations are limited by the growth of entanglement [63]. Despite notable progress to extend these time scales [53,57] and the development of other sophisticated methods [64–66], studying quantum many-body dynamics, especially beyond 1D, remains difficult [67–69].

In this Letter, we study the nature of the MBL regime in two classes of disordered models (see Fig. 1), (i) spin-1/2 two-leg ladders [53,70–72], a quasi-1D system, which represents an intermediate case between a 1D chain and a 2D lattice, and (ii) Fermi-Hubbard (FH) chains [73–79], where disorder only couples to the charge degrees of freedom. Both can also be viewed as 1D models with local Hilbert-space dimension greater than two. In the FH chain, there is a SU(2) symmetry incompatible with MBL, and we also study the effect of a tilted potential which can induce Stark MBL [44,45,80].

We demonstrate that numerical linked cluster expansions (NLCE) [81] provide a powerful means to study the MBL regime. The crucial advantage of NLCE is that, if converged, they yield results directly in the thermodynamic limit, i.e., there are no finite-size effects. We use NLCE to study the dynamics resulting from out-of-equilibrium initial states and obtain converged results for the imbalance $\mathcal{I}(t)$ on long time

*j.richter@ucl.ac.uk
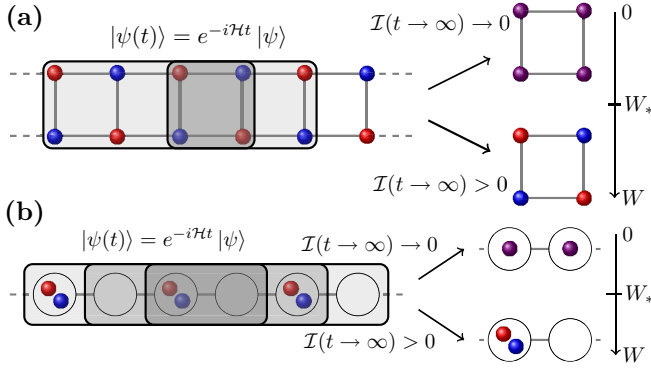
FIG. 1. We study the imbalance $\mathcal{I}(t)$ in disordered **(a)** two-leg spin ladders and **(b)** FH chains. (Disorder not shown here.) For $W < W_*$, $\mathcal{I}(t)$ is expected to decay to zero, while $\mathcal{I}(t) > 0$ in the MBL phase for $W > W_*$. NLCE is used to simulate $\mathcal{I}(t)$ in the thermodynamic limit $L \to \infty$. Within NLCE, $\mathcal{I}(t)$ is obtained on finite clusters (shaded rectangles), whose contributions are suitably combined to yield quantum dynamics without finite-size effects [107].

scales, outperforming direct simulations of finite systems with open or periodic boundaries especially for intermediate disorder $W < W_*$, which allows the extraction of more accurate lower bounds for W_*. Furthemore, we show that, in contrast to strongly disordered FH chains where spin thermalizes despite charge being localized, an additional tilted potential leads to a slowdown of the spin imbalance and nonergodic behavior for certain initial states.

Models and Observables.– The first class of models we consider are disordered Heisenberg two-leg spin ladders,

$$\mathcal{H}_{\text{SL}} = \sum_{k=1}^{2} \sum_{\ell} \left(\mathbf{S}_{\ell,k} \mathbf{S}_{\ell+1,k} + h_{\ell,k} S_{\ell,k}^z \right) + \sum_{\ell=1}^{L} \mathbf{S}_{\ell,1} \cdot \mathbf{S}_{\ell,2}, \quad (1)$$

where $\mathbf{S}_{\ell,k} = (S_{\ell,k}^x, S_{\ell,k}^y, S_{\ell,k}^z)$ are spin-1/2 operators on leg k and rung ℓ, L denotes the length of the ladder ($2L$ lattice sites in total), and the on-site fields $h_{\ell,k} \in [-W, W]$ are randomly drawn from a uniform distribution with W setting the strength of disorder. We study the nonequilibrium dynamics resulting from quenches with antiferromagnetic initial states of the form [cf. Fig. 1(a)],

$$|\psi(0)\rangle = \begin{vmatrix} \cdots & \downarrow & \uparrow & \downarrow & \uparrow & \downarrow & \uparrow & \cdots \\ \cdots & \uparrow & \downarrow & \uparrow & \downarrow & \uparrow & \downarrow & \cdots \end{vmatrix}, \quad (2)$$

in the $\sum_{k,\ell} S_{\ell,k}^z = 0$ sector. We monitor the imbalance, $\mathcal{I}(t) = \sum_k \sum_\ell (-1)^{k+\ell} \langle S_{\ell,k}^z(t) \rangle / L$, where $\langle \cdot(t) \rangle = \langle \psi(t)| \cdot |\psi(t)\rangle$, $|\psi(t)\rangle = e^{-i\mathcal{H}t}|\psi(0)\rangle$, and $\mathcal{I}(0) = 1$. In case of thermalization, one expects $\lim_{t\to\infty} \lim_{L\to\infty} \mathcal{I}(t) \to 0$. In contrast, $\mathcal{I}(t) > 0$ in the case of MBL, see Fig. 1. Distinguishing between asymptotically localized or delocalized dynamics is challenging due to (i) finite-size effects and (ii) finite simulation times. In this Letter, we show that NLCE provides a means to mitigate the impact of (i) by obtaining $\mathcal{I}(t)$ in the thermodynamic limit $L \to \infty$.

As a second model, we study disordered FH chains,

$$\mathcal{H}_{\text{FH}} = -\sum_{\ell,\sigma}(c_{\ell,\sigma}^\dagger c_{\ell+1,\sigma} + \text{H.c.}) + \sum_{\ell=1}^{L}(U n_{\ell,\uparrow} n_{\ell,\downarrow} + \mu_\ell n_\ell), \quad (3)$$

where $c_{\ell,\sigma}^\dagger$ ($c_{\ell,\sigma}$) creates (annihilates) a fermion of spin σ at site ℓ, U is the on-site interaction; $n_{\ell,\sigma} = c_{\ell,\sigma}^\dagger c_{\ell,\sigma}$, $n_\ell = n_{\ell,\uparrow} + n_{\ell,\downarrow}$; and $\mu_\ell = \epsilon_\ell + V\ell$ with $\epsilon_\ell \in [-W, W]$ is the spin-independent disorder with added tilt V [44,45,82–85]. In our implementation, we exploit that $\mathcal{H}_{\text{FH}}$ can be mapped to a spin ladder, where the interactions are mediated by the rungs of the ladder [48,86].

We consider two experimentally relevant initial states [82,87], i.e., density waves at half filling [cf. Fig. 1(b)],

$$|\psi_1(0)\rangle = \prod_\ell c_{2\ell,\uparrow}^\dagger c_{2\ell,\downarrow}^\dagger |0\rangle = |\cdots \quad \uparrow\downarrow \quad 0 \quad \uparrow\downarrow \quad 0 \quad \cdots\rangle, \quad (4)$$

or at quarter filling [74], both at zero magnetization,

$$|\psi_2(0)\rangle = \prod_\ell c_{4\ell,\uparrow}^\dagger c_{4\ell+2,\downarrow}^\dagger |0\rangle = |\cdots \quad \uparrow \quad 0 \quad \downarrow \quad 0 \quad \cdots\rangle. \quad (5)$$

We simulate the charge and spin imbalances, $\mathcal{I}_{\text{ch}}(t) \propto \sum_\ell \langle n_\ell(t) \rangle \langle n_\ell(0) \rangle$ and $\mathcal{I}_{\text{s}}(t) \propto \sum_\ell \langle m_\ell(t) \rangle \langle m_\ell(0) \rangle$, with $m_\ell = n_{\ell,\uparrow} - n_{\ell,\downarrow}$, and $\mathcal{I}_{\text{ch(s)}}(0) = 1$ [88].

While we are mainly interested in $\mathcal{I}(t)$ in the thermodynamic limit $L \to \infty$ using NLCE, we also consider finite systems with periodic boundary conditions (PBC) or open boundary conditions (OBC). For PBC, the first sums in Eqs. (1) and (3) run from $\ell = 1$ to $\ell = L$, with $\mathbf{S}_{L+1,k} = \mathbf{S}_{1,k}$, $c_{L+1,\sigma}^{(\dagger)} = c_{1,\sigma}^{(\dagger)}$, while in the case of OBC they run up to $\ell = L - 1$. As explained below, systems with OBC are a main ingredient within the NLCE formalism.

NLCE.– NLCE provides a means to study quantum systems directly in the thermodynamic limit $L \to \infty$. The main idea is to write the quantity of interest as a sum over contributions from all clusters that can be embedded on the lattice [81,89]. Originally introduced in the context of thermodynamics [90], NLCE has also been used to study open quantum systems [91], entanglement entropies [92], dynamical correlation functions [93–95], and quantum quenches in 1D and 2D systems [96–101]. While NLCE are usually formulated for translational invariant systems, disordered systems can be treated as well [102–106], albeit with higher computational costs (as discussed below). In fact, NLCE has been used to study models with discrete disorder where an exact disorder averaging can be performed [102–104]. Moreover, it was demonstrated that NLCE allows for a more accurate estimation of the critical disorder W_* in the disordered Heisenberg chain [105]. This approach was then adapted to study nonequilibrium dynamics of inhomogeneous systems [106]. Building on Ref. [106], we here demonstrate that NLCE can provide insights into the localization and delocalization dynamics in (quasi-)1D models, such as $\mathcal{H}_{\text{SL}}$ and $\mathcal{H}_{\text{FH}}$, by giving access to the imbalance $\mathcal{I}(t)$ for $L \to \infty$ (see also Supplemental Material [107]). To this end, we consider an infinite system with a random disorder realization and define a unit cell ●, e.g., a spin plaquette or two neighboring lattice sites; see Fig. 1. For a given cluster c, let $\mathcal{P}_c(t)$ be the

sum [106],

$$\mathcal{P}_c(t) = \sum_{\mathcal{T}(c),\,\bullet\!-\subset\mathcal{T}(c)} [\mathcal{I}_{\bullet\!-}(t)]_{\mathcal{T}(c)} \qquad (6)$$

which runs over all translations $\mathcal{T}(c)$ of c such that $\bullet\!-$ is included in $\mathcal{T}(c)$, and $[\mathcal{I}_{\bullet\!-}(t)]_{\mathcal{T}(c)}$ denotes the local unit-cell imbalance evaluated on $\mathcal{T}(c)$ [106,107]. The notion of a cluster here refers to a finite part of the full system with OBC. Given the (quasi-)1D geometries of $\mathcal{H}_{SL}$ and $\mathcal{H}_{FH}$, clusters are just ladders or chains of varying size [94,99,108] (cf. gray rectangles in Fig. 1). Due to the presence of disorder, $[\mathcal{I}_{\bullet\!-}(t)]_{\mathcal{T}(c)}$ is nonequivalent for different translations. The weight of c is then given by an inclusion-exclusion principle [81,106],

$$\mathcal{W}_c(t) = \mathcal{P}_c(t) - \sum_{\mathcal{T}(c')\subset\mathcal{T}(c)} \mathcal{W}_{c'}(t), \qquad (7)$$

where the sum runs over all subclusters c' of c (and their translations) that include $\bullet\!-$. The unit cell provides the starting point and has no subclusters such that $\mathcal{W}_{\bullet\!-}(t) = \mathcal{I}_{\bullet\!-}(t)$. The dynamics of the imbalance $\mathcal{I}(t)$ in the thermodynamic limit can then be approximated as

$$\lim_{L\to\infty} \mathcal{I}(t) \approx \sum_{|c|\leqslant c_{\max}} \mathcal{W}_c(t), \qquad (8)$$

including all clusters c up to a cutoff size $|c| = c_{\max}$ that can be handled numerically. While NLCE yields results in the thermodynamic limit, i.e., there are no finite-size effects, one instead has to check the convergence of Eq. (8) with respect to the expansion order $c_{\max}$, which acts as an effective length scale. Typically, a larger $c_{\max}$ leads to convergence on longer time scales [93,99] (or down to lower temperatures [81,109,110]). Reaching large $c_{\max}$ is computationally costly for multiple reasons. First, using full exact diagonalization (ED) to evaluate Eqs. (6)–(8) is limited to rather small cluster sizes due to the exponentially growing Hilbert space. Here we employ an efficient sparse-matrix approach based on Chebyshev polynomials [111–113] to evaluate $e^{-i\mathcal{H}t}|\psi\rangle$ beyond the range of ED [93,94], which yields a high accuracy even at long times [107]. Second, in the pertinent case of disordered systems, all $\sim|c|$ translations of a given cluster of size $|c|$ have to be simulated. Due to this computational overhead compared with NLCE in translational-invariant models, we (mostly) consider expansion orders up to $c_{\max} = 11$, which means that the largest clusters in our simulations are ladders of length $L = 11$ (or FH chains with $L = 11$). While even larger clusters could in principle be simulated using the sparse-matrix approach, we find that this $c_{\max}$ leads to a reasonable trade-off between the invested computational effort and the time scales on which the NLCE remains converged. In addition to this main bottleneck of NLCE to reach sufficiently large $c_{\max}$, the costs are further increased by the necessity to perform an average over N_s independent disorder samples (here $N_s \approx 10^3$).

MBL in spin ladders.– We now present our numerical results, starting with $\mathcal{H}_{SL}$ and the initial state in Eq. (2). In Figs. 2(a) and 2(b), the imbalance $\mathcal{I}(t)$ is shown for disorder strengths $W = 2$ and $W = 4$. Data obtained by NLCE for
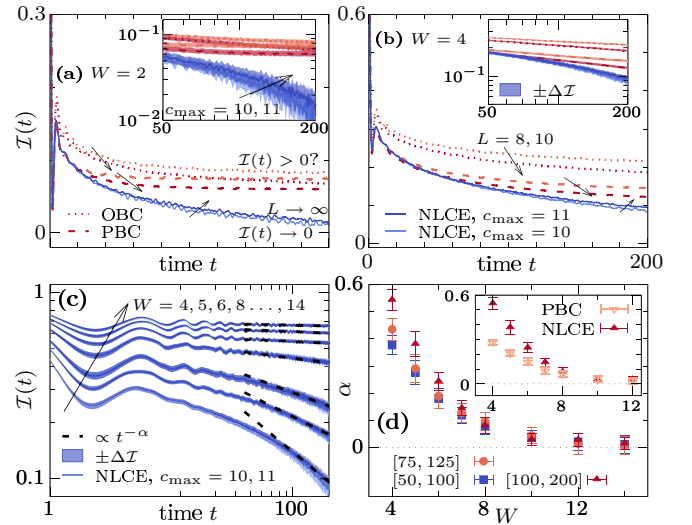
FIG. 2. $\mathcal{I}(t)$ in disordered spin ladders (1). **[(a), (b)]** Data for $W = 2, 4$ obtained by NLCE for $c_{\max} = 10, 11$ (solid) are compared with simulations of finite systems with $L = 8, 10$ with OBC (dotted) and PBC (dashed). Direction of increasing L ($c_{\max}$) is indicated by arrows. **Insets:** Same data but in a double-logarithmic plot. Shaded area indicates standard error $\Delta\mathcal{I}$ of the mean [114]. **(c)** $\mathcal{I}(t)$ for different W (arrow). At long times, $\mathcal{I}(t) \propto t^{-\alpha}$. **(d)** Exponent α extracted from fitting data in (c) in different time windows. **Inset:** α obtained by NLCE ($c_{\max} = 10$) and PBC ($L = 10$) for $t \in [100, 200]$. Data are averaged over $N_s \approx 10^3$ disorder realizations.

expansion orders $c_{\max} = 10, 11$ (solid curves) are compared with simulations of finite ladders of length $L = 8, 10$ with OBC (dotted) or PBC (dashed). While the $L \to \infty$ dynamics from NLCE remain converged up to the longest time $t = 200$ simulated here (see Ref. [107] for additional analysis of convergence), we find that $\mathcal{I}(t)$ in the case of $L < \infty$ shows finite-size effects already at early times (particularly for OBC). Especially at $W = 2$ [Fig. 2(a)], $\mathcal{I}(t)$ obtained by NLCE decays to a rather small value, with a slope that indicates that the system will delocalize at long times. In contrast, in the case of finite systems, $\mathcal{I}(t)$ decays to notably higher values, with the slope of $\mathcal{I}(t)$ being less pronounced. Compared with the $L \to \infty$ NLCE results, extrapolating these finite-system data to longer t and larger L is thus more intricate and it is less clear whether $\mathcal{I}(t)$ eventually vanishes. This example demonstrates a main result of this Letter. In particular, employing NLCE to obtain quantum dynamics for $L \to \infty$ can be a powerful means to decide whether a system is asymptotically localized or delocalized. Let us note that this regime of intermediate disorder is expected to be challenging also for other more sophisticated techniques, such as matrix-product states, since entanglement presumably still grows rather rapidly.

A similar picture also emerges for $W = 4$ [Fig. 2(b)]. However, as the dynamics are slower and finite-size effects are smaller (at least on the time scales shown here), the advantage of NLCE compared with direct simulations of finite systems becomes less pronounced. Moreover, as emphasized in the insets of Figs. 2(a) and 2(b), the dynamics of $\mathcal{I}(t)$ obtained by NLCE are more noisy compared with the data for PBC or OBC. This is caused by the fact that NLCE relies on the local
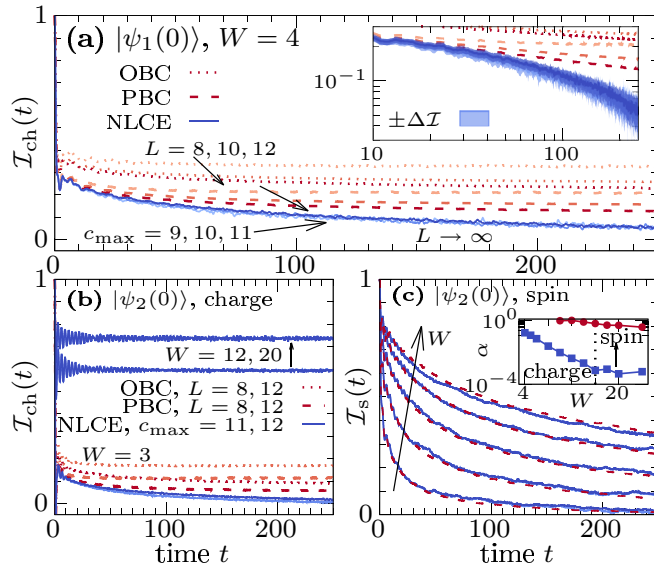
FIG. 3. Dynamics in $\mathcal{H}_{FH}$ with $U = 4$ and $V = 0$. **(a)** $\mathcal{I}_{ch}(t)$ for $|\psi_1(0)\rangle$ at $W = 4$ obtained by NLCE for $c_{max} \leqslant 11$ (solid) and for finite systems with OBC (dotted) and PBC (dashed) and $L = 8, 10, 12$ (arrow). **Inset:** Same data but in a double-logarithmic plot. **(b)** $\mathcal{I}_{ch}(t)$ for $|\psi_2(0)\rangle$ for different W. **(c)** $\mathcal{I}_s(t)$ for $|\psi_2(0)\rangle$ at $W = 8, 12, \ldots, 24$ (arrow) using NLCE ($c_{max} = 11, 12$; converged) and systems with OBC ($L = 12$). **Inset:** α obtained by fitting $\mathcal{I}_{ch}(t)$ and $\mathcal{I}_s(t)$ for $t \in [150, 250]$.

unit-cell imbalance $[\mathcal{I}_{\bullet}(t)]_{\mathcal{T}(c)}$ [107], whereas $\mathcal{I}(t)$ in finite systems is averaged over the full length of the system. While the increased noise in the NLCE data may especially affect the short-time dynamics, we expect it to be less relevant for the qualitative long-time behavior of $\mathcal{I}(t)$.

To proceed, Fig. 2(c) shows $\mathcal{I}(t)$ for various disorder strengths up to $W = 14$. While the NLCE data for $c_{max} = 9, 10$ remain well converged, we observe that $\mathcal{I}(t)$ can be described by a power law [56,57],

$$\mathcal{I}(t) \propto t^{-\alpha}, \tag{9}$$

with α depending on W. We extract α for varying time windows and show the corresponding data in Fig. 2(d). Since one expects $\alpha \to 0$ in the localized phase, Fig. 2(d) suggests a critical disorder for $\mathcal{H}_{SL}$ of $W_* \gtrsim 14$, which is notably higher than for the disordered Heisenberg chain [10,57,105], consistent with $\mathcal{H}_{SL}$ being an intermediate case between 1D and 2D [53]. As shown in the inset of Fig. 2(d), extracting α from the dynamics of finite systems with PBC and $L = 10$ leads to systematically lower values of α (especially for $W \lesssim 8$). Obtaining α from NLCE simulations for $L \to \infty$ thus facilitates an accurate estimation of W_*, in line with earlier NLCE studies of eigenstate entanglement entropies [105].

MBL in FH chains.– We now turn to the dynamics of $\mathcal{H}_{FH}$. We fix the interaction to $U = 4$ and, for now, focus on the nontilted model, $V = 0$. Figure 3(a) shows the charge imbalance $\mathcal{I}_{ch}(t)$ for the initial state $|\psi_1(0)\rangle$ (4) at $W = 4$, where we again compare the dynamics obtained by NLCE to simulations of finite systems with OBC and PBC. Similar to our previous observations in the context of
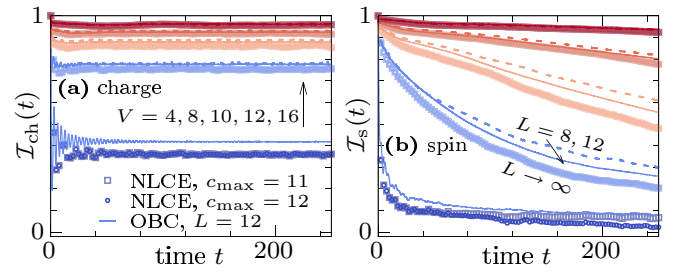
FIG. 4. **(a)** $\mathcal{I}_{ch}(t)$ and **(b)** $\mathcal{I}_s(t)$ for $|\psi_2(0)\rangle$ at fixed $W = 4$, $U = 4$, and different lattice tilts $V \leqslant 16$. Data for chains with OBC and $L = 8, 12$ (dashed, solid) are compared with $L \to \infty$ NLCE dynamics with $c_{max} = 11, 12$ (squares, circles). NLCE remains well converged except for $\mathcal{I}_s(t)$ and $V = 4$.

$\mathcal{H}_{SL}$, we find that NLCE yields converged dynamics on long time scales with a pronounced decay of $\mathcal{I}_{ch}(t)$ consistent with delocalization. In contrast, the relaxation of $\mathcal{I}_{ch}(t)$ for $L < \infty$ is slower and finite-size effects appear at early times [cf. inset in Fig. 3(a)]. We stress that for the highest $c_{max} = 11$ considered here, the largest clusters are chains with OBC and $L = 11$ [107]. Nevertheless, Fig. 3(a) unveils that combining the contributions of the clusters according to Eqs. (6)–(8) outperforms direct simulations of systems with OBC and PBC up to $L = 12$, even though the length scales are comparable. NLCE thus proves advantageous also in the case of moderately disordered FH chains.

Next, we consider the initial state $|\psi_2(0)\rangle$ in Eq. (5) with $\mathcal{I}_{ch}(t)$ shown in Fig. 3(b) for exemplary values of W. While we observe delocalized dynamics for $W = 3$, most pronounced in the case of the $L \to \infty$ NLCE data, $\mathcal{I}_{ch}(t) > 0$ approaches approximately time-independent plateaus for $W = 12, 20$, suggesting charge localization at sufficiently strong disorder, cf. inset in Fig. 3(c). While nonergodic charge dynamics have been observed before [73,74], spin was found to be delocalized and relax subdiffusively instead [75]. Here we explore the fate of spin dynamics for $L \to \infty$ at strong disorder. Specifically, the spin imbalance $\mathcal{I}_s(t)$ is shown in Fig. 3(c) for $W \leqslant 24$. Using NLCE up to $c_{max} = 12$ [115], we find no signatures of localization and $\mathcal{I}_s(t)$ decays as $\propto t^{-\alpha}, \alpha > 0$ [inset in Fig. 3(c)]. The fact that the $L \to \infty$ dynamics obtained by NLCE and for systems with $L = 12$ agree very well with each other demonstrates that finite-size effects are negligible. Spin dynamics of $\mathcal{H}_{FH}$ thus behave delocalized even at extremely large W, where charge is frozen.

Dynamics in tilted lattice.– We now consider $\mathcal{H}_{FH}$ with $V > 0$. While such tilts may lead to Stark localization [44,45,80], nonergodic dynamics in strongly tilted lattices has also been attributed to Hilbert-space fragmentation [82,116–118]. Fixing the disorder to $W = 4$ (for which $\mathcal{H}_{FH}$ is delocalized at $V = 0$, cf. Fig. 3), Figure 4 shows $\mathcal{I}_{ch}(t)$ and $\mathcal{I}_s(t)$ resulting from quenches with $|\psi_2(0)\rangle$ and different $V > 0$ obtained by NLCE for $L \to \infty$ and direct simulations of finite chains with OBC. While $W > 0$ is convenient to suppress the strong oscillations of $\mathcal{I}(t)$ [107], the combination of disorder and lattice tilt may reinforce localization [45]. Remarkably, we observe in Fig. 4 that not only $\mathcal{I}_{ch}(t)$ ceases to decay with increasing V but also $\mathcal{I}_s(t)$ slows down drastically with V,

especially compared with the case of bare disorder and no tilt [cf. Fig. 3(c)]. In particular, for the largest $V = 16$ considered here, $\mathcal{I}_s(t)$ does not substantially decay for $t < 250$, suggesting the possibility to induce nonergodic spin dynamics on experimentally relevant time scales in tilted lattices. This is another key result. We stress that this mechanism of causing slow spin dynamics is distinct from other examples where localization was achieved by lifting the SU(2) symmetry of $\mathcal{H}_{FH}$ [119]. While $\mathcal{I}_s(t)$ appears to be strongly initial-state dependent (see Ref. [107]), we here leave it to future work to explore the effect of $V > 0$ in more detail.

Conclusion.– To summarize, we have employed NLCE to study quantum quenches in disordered spin ladders and FH chains and obtained converged results for the imbalance $\mathcal{I}(t)$ on comparatively long time scales. We have put particular emphasis on intermediate disorder values $W < W_*$, where we demonstrated that NLCE outperforms direct simulations of finite systems with OBC or PBC. Furthermore, in contrast with bare disorder, our analysis predicts that an additional tilted potential leads to a notable slowdown of spin dynamics for certain initial states in FH chains, which should be accessible experimentally [82]. Even though NLCE yields results for $L \to \infty$, allowing better estimates for W_* [105], we stress that, similar to other methods, an unambiguous detection of MBL is beyond its capabilities (and was not our goal). Since simulation times are limited, $t < \infty$, extracted values for W_* should be understood as lower bounds for the putative MBL transition.

Given the apparent advantage of NLCE at intermediate disorder, a natural direction of research is to explore the emergence of subdiffusion on the ergodic side of the MBL transition [23,54,120,121]. In this context, NLCE have been shown to be a powerful means to study transport properties of 1D systems in the thermodynamic limit [93]. Another interesting avenue is to consider MBL in higher dimensions. While NLCE has proven competitive with other state-of-the-art methods to simulate quantum dynamics in 2D [101], reaching high expansion orders for 2D lattices is computationally demanding such that convergence times are still limited [106].

[1] R. Nandkishore and D. A. Huse, Annu. Rev. Condens. Matter Phys. **6**, 15 (2015).

[2] D. A. Abanin, E. Altman, I. Bloch, and M. Serbyn, Rev. Mod. Phys. **91**, 021001 (2019).

[3] I. V. Gornyi, A. D. Mirlin, and D. G. Polyakov, Phys. Rev. Lett. **95**, 206603 (2005).

[4] D. M. Basko, I. L. Aleiner, and B. L. Altshuler, Ann. Phys. **321**, 1126 (2006).

[5] V. Oganesyan and D. A. Huse, Phys. Rev. B **75**, 155111 (2007).

[6] A. Pal and D. A. Huse, Phys. Rev. B **82**, 174411 (2010).

[7] J. A. Kjäll, J. H. Bardarson, and F. Pollmann, Phys. Rev. Lett. **113**, 107204 (2014).

[8] J. Z. Imbrie, Phys. Rev. Lett. **117**, 027201 (2016).

[9] T. C. Berkelbach and D. R. Reichman, Phys. Rev. B **81**, 224429 (2010).

[10] D. J. Luitz, N. Laflorencie, and F. Alet, Phys. Rev. B **91**, 081103(R) (2015).

[11] S. Bera, H. Schomerus, F. Heidrich-Meisner, and J. H. Bardarson, Phys. Rev. Lett. **115**, 046603 (2015).

[12] L. D'Alessio, Y. Kafri, A. Polkovnikov, and M. Rigol, Adv. Phys. **65**, 239 (2016).

[13] B. Bauer and C. Nayak, J. Stat. Mech. (2013) P09005.

[14] M. Žnidarič, T. Prosen, and P. Prelovšek, Phys. Rev. B **77**, 064426 (2008).

[15] J. H. Bardarson, F. Pollmann, and J. E. Moore, Phys. Rev. Lett. **109**, 017202 (2012).

[16] M. Serbyn, Z. Papić, and D. A. Abanin, Phys. Rev. Lett. **111**, 127201 (2013).

[17] D. A. Huse, R. Nandkishore, and V. Oganesyan, Phys. Rev. B **90**, 174202 (2014).

[18] A. Chandran, I. H. Kim, G. Vidal, and D. A. Abanin, Phys. Rev. B **91**, 085425 (2015).

[19] V. Ros, M. Müller, and A. Scardicchio, Nucl. Phys. B **891**, 420 (2015).

[20] M. Schreiber, S. S. Hodgman, P. Bordia, H. P. Lüschen, M. H. Fischer, R. Vosk, E. Altman, U. Schneider, and I. Bloch, Science **349**, 842 (2015).

[21] J.-y. Choi, S. Hild, J. Zeiher, P. Schauß, A. Rubio-Abadal, T. Yefsah, V. Khemani, D. A. Huse, I. Bloch, and C. Gross, Science **352**, 1547 (2016).

[22] J. Smith, A. Lee, P. Richerme, B. Neyenhuis, P. W. Hess, P. Hauke, M. Heyl, D. A. Huse, and C. Monroe, Nat. Phys. **12**, 907 (2016).

[23] D. J. Luitz and Y. Bar Lev, Ann. Phys. **529**, 1600350 (2017).

[24] T. Enss, F. Andraschko, and J. Sirker, Phys. Rev. B **95**, 045121 (2017).

[25] A. Nico-Katz, A. Bayat, and S. Bose, arXiv:2111.01146 (2021).

[26] T. B. Wahl, A. Pal, and S. H. Simon, Nat. Phys. **15**, 164 (2019).

[27] K. S. C. Decker, D. M. Kennes, and C. Karrasch, arXiv:2106.12861.

[28] E. Chertkov, B. Villalonga, and B. K. Clark, Phys. Rev. Lett. **126**, 180602 (2021).

[29] A. C. Potter and R. Vasseur, Phys. Rev. B **94**, 224206 (2016).

[30] I. V. Protopopov, W. W. Ho, and D. A. Abanin, Phys. Rev. B **96**, 041122(R) (2017).

[31] S. A. Parameswaran and R. Vasseur, Rep. Prog. Phys. **81**, 082501 (2018).

[32] I. V. Protopopov, R. K. Panda, T. Parolini, A. Scardicchio, E. Demler, and D. A. Abanin, Phys. Rev. X **10**, 011025 (2020).

[33] R. M. Nandkishore and S. L. Sondhi, Phys. Rev. X **7**, 041021 (2017).

[34] N. Y. Yao, C. R. Laumann, S. Gopalakrishnan, M. Knap, M. Müller, E. A. Demler, and M. D. Lukin, Phys. Rev. Lett. **113**, 243002 (2014).

[35] A. L. Burin, Phys. Rev. B **91**, 094202 (2015).

[36] R. Modak and T. Nag, Phys. Rev. E **101**, 052108 (2020).

[37] J. Richter, N. Casper, W. Brenig, and R. Steinigeweg, Phys. Rev. B **100**, 144423 (2019).

[38] J. Richter, D. Schubert, and R. Steinigeweg, Phys. Rev. Res. **2**, 013130 (2020).

[39] J. Schliemann, J. V. I. Costa, P. Wenk, and J. C. Egues, Phys. Rev. B **103**, 174203 (2021).

[40] T. Grover and M. P. A. Fisher, J. Stat. Mech. (2014) P10010.

[41] M. Schiulaz and M. Müller, in *15th International Conference on Transport in Interacting Disordered Systems (TIDS15)*, edited by M. Palassini, AIP Conf. Proc. No. 1610 (AIP, New York, 2014), p. 11.

[42] N. Y. Yao, C. R. Laumann, J. I. Cirac, M. D. Lukin, and J. E. Moore, Phys. Rev. Lett. **117**, 240601 (2016).

[43] J. Sirker, Phys. Rev. B **99**, 075162 (2019).

[44] M. Schulz, C. A. Hooley, R. Moessner, and F. Pollmann, Phys. Rev. Lett. **122**, 040606 (2019).

[45] E. van Nieuwenburg, Y. Baum, and G. Refael, Proc. Natl. Acad. Sci. USA **116**, 9269 (2019).

[46] A. Smith, J. Knolle, D. L. Kovrizhin, and R. Moessner, Phys. Rev. Lett. **118**, 266601 (2017).

[47] M. Brenes, M. Dalmonte, M. Heyl, and A. Scardicchio, Phys. Rev. Lett. **120**, 030601 (2018).

[48] T. Heitmann, J. Richter, T. Dahm, and R. Steinigeweg, Phys. Rev. B **102**, 045137 (2020).

[49] P. Karpov, R. Verdel, Y.-P. Huang, M. Schmitt, and M. Heyl, Phys. Rev. Lett. **126**, 130401 (2021).

[50] S. Gopalakrishnan and S. A. Parameswaran, Phys. Rep. **862**, 1 (2020).

[51] A. Morningstar, L. Colmenarez, V. Khemani, D. J. Luitz, and D. A. Huse, Phys. Rev. B **105**, 174205 (2022).

[52] W. De Roeck and F. Huveneers, Phys. Rev. B **95**, 155129 (2017).

[53] E. V. H. Doggen, I. V. Gornyi, A. D. Mirlin, and D. G. Polyakov, Phys. Rev. Lett. **125**, 155701 (2020).

[54] F. Weiner, F. Evers, and S. Bera, Phys. Rev. B **100**, 104204 (2019).

[55] R. K. Panda, A. Scardicchio, M. Schulz, S. R. Taylor, and M. Žnidarič, Europhys. Lett. **128**, 67003 (2020).

[56] P. Sierant and J. Zakrzewski, Phys. Rev. B **105**, 224203 (2022).

[57] E. V. H. Doggen, F. Schindler, K. S. Tikhonov, A. D. Mirlin, T. Neupert, D. G. Polyakov, and I. V. Gornyi, Phys. Rev. B **98**, 174202 (2018).

[58] D. A. Abanin, J. H. Bardarson, G. De Tomasi, S. Gopalakrishnan, V. Khemani, S. A. Parameswaran, F. Pollmann, A. C. Potter, M. Serbyn, and R. Vasseur, Ann. Phys. **427**, 168415 (2021).

[59] P. Sierant, M. Lewenstein, and J. Zakrzewski, Phys. Rev. Lett. **125**, 156601 (2020).

[60] J. Šuntajs, J. Bonča, T. Prosen, and L. Vidmar, Phys. Rev. E **102**, 062144 (2020).

[61] M. Kiefer-Emmanouilidis, R. Unanyan, M. Fleischhauer, and J. Sirker, Phys. Rev. Lett. **124**, 243601 (2020).

[62] D. Sels and A. Polkovnikov, Phys. Rev. E **104**, 054105 (2021).

[63] S. Paeckel, T. Köhler, A. Swoboda, S. R. Manmana, U. Schollwöck, and C. Hubig, Ann. Phys. **411**, 167998 (2019).

[64] H. Burau and M. Heyl, Phys. Rev. Lett. **127**, 050601 (2021).

[65] S. J. Thomson and M. Schiró, Phys. Rev. B **97**, 060201(R) (2018).

[66] T. K. Kvorning, L. Herviou, and J. H. Bardarson, arXiv:2105.11206.

[67] D. M. Kennes, arXiv:1811.04126.

[68] C. Hubig and J. I. Cirac, SciPost Phys. **6**, 031 (2019).

[69] A. Kshetrimayum, M. Goihl, and J. Eisert, Phys. Rev. B **102**, 235132 (2020).

[70] E. Baygan, S. P. Lim, and D. N. Sheng, Phys. Rev. B **92**, 195153 (2015).

[71] D. Wiater and J. Zakrzewski, Phys. Rev. B **98**, 094202 (2018).

[72] J. Hauschild, F. Heidrich-Meisner, and F. Pollmann, Phys. Rev. B **94**, 161109(R) (2016).

[73] P. Prelovšek, O. S. Barišić, and M. Žnidarič, Phys. Rev. B **94**, 241104(R) (2016).

[74] R. Mondaini and M. Rigol, Phys. Rev. A **92**, 041601(R) (2015).

[75] M. Kozarzewski, P. Prelovšek, and M. Mierzejewski, Phys. Rev. Lett. **120**, 246602 (2018).

[76] J. Zakrzewski and D. Delande, Phys. Rev. B **98**, 014203 (2018).

[77] T. Iadecola and M. Žnidarič, Phys. Rev. Lett. **123**, 036403 (2019).

[78] I. V. Protopopov and D. A. Abanin, Phys. Rev. B **99**, 115111 (2019).

[79] D. V. Kurlov, M. S. Bahovadinov, S. I. Matveenko, A. K. Fedorov, V. Gritsev, B. L. Altshuler, and G. V. Shlyapnikov, arXiv:2112.06895.

[80] Q. Guo, C. Cheng, H. Li, S. Xu, P. Zhang, Z. Wang, C. Song, W. Liu, W. Ren, H. Dong, R. Mondaini, and H. Wang, Phys. Rev. Lett. **127**, 240502 (2021).

[81] B. Tang, E. Khatami, and M. Rigol, Comput. Phys. Commun. **184**, 557 (2013).

[82] S. Scherg, T. Kohlert, P. Sala, F. Pollmann, B. H. Madhusudhana, I. Bloch, and M. Aidelsburger, Nat. Commun. **12**, 4490 (2021).

[83] E. Guardado-Sanchez, A. Morningstar, B. M. Spar, P. T. Brown, D. A. Huse, and W. S. Bakr, Phys. Rev. X **10**, 011042 (2020).

[84] R. Yao, T. Chanda, and J. Zakrzewski, Ann. Phys. **435**, 168540 (2021).

[85] J.-Y. Desaules, A. Hudomal, C. J. Turner, and Z. Papić, Phys. Rev. Lett. **126**, 210601 (2021).

[86] T. Prosen and M. Žnidarič, Phys. Rev. B **86**, 125118 (2012).

[87] S. Scherg, T. Kohlert, J. Herbrych, J. Stolpp, P. Bordia, U. Schneider, F. Heidrich-Meisner, I. Bloch, and M. Aidelsburger, Phys. Rev. Lett. **121**, 130402 (2018).

[88] For $|\psi_1(0)\rangle$, $\mathcal{I}_s(0) = 0$ and we focus on $\mathcal{I}_{ch}(t)$ in this case.

[89] S. Dusuel, M. Kamfor, K. P. Schmidt, R. Thomale, and J. Vidal, Phys. Rev. B **81**, 064412 (2010).

[90] M. Rigol, T. Bryant, and R. R. P. Singh, Phys. Rev. Lett. **97**, 187202 (2006).

[91] A. Biella, J. Jin, O. Viyuela, C. Ciuti, R. Fazio, and D. Rossini, Phys. Rev. B **97**, 035103 (2018).

[92] A. B. Kallin, K. Hyatt, R. R. P. Singh, and R. G. Melko, Phys. Rev. Lett. **110**, 135702 (2013).

[93] J. Richter and R. Steinigeweg, Phys. Rev. B **99**, 094419 (2019).

[94] J. Richter, F. Jin, L. Knipschild, H. De Raedt, K. Michielsen, J. Gemmer, and R. Steinigeweg, Phys. Rev. E **101**, 062133 (2020).

[95] T. Heitmann, J. Richter, J. Gemmer, and R. Steinigeweg, Phys. Rev. E **104**, 054145 (2021).

[96] I. G. White, B. Sundar, and K. R. A. Hazzard, arXiv:1710.07696.

[97] B. Wouters, J. De Nardis, M. Brockmann, D. Fioretto, M. Rigol, and J.-S. Caux, Phys. Rev. Lett. **113**, 117202 (2014).

[98] K. Mallayya and M. Rigol, Phys. Rev. E **95**, 033302 (2017).

[99] K. Mallayya and M. Rigol, Phys. Rev. Lett. **120**, 070603 (2018).

[100] E. Guardado-Sanchez, P. T. Brown, D. Mitra, T. Devakul, D. A. Huse, P. Schauß, and W. S. Bakr, Phys. Rev. X **8**, 021069 (2018).

[101] J. Richter, T. Heitmann, and R. Steinigeweg, SciPost Phys. **9**, 031 (2020).

[102] B. Tang, D. Iyer, and M. Rigol, Phys. Rev. B **91**, 161109(R) (2015).

[103] M. D. Mulanix, D. Almada, and E. Khatami, Phys. Rev. B **99**, 205113 (2019).

[104] J. Park and E. Khatami, Phys. Rev. B **104**, 165102 (2021).

[105] T. Devakul and R. R. P. Singh, Phys. Rev. Lett. **115**, 187201 (2015).

[106] J. Gan and K. R. A. Hazzard, Phys. Rev. A **102**, 013318 (2020).

[107] See Supplemental Material at http://link.aps.org/supplemental/10.1103/PhysRevB.105.L220405 for details on NLCEs for disordered systems, the forward propagation of pure states using Chebyshev polynomials, the convergence properties, and the accuracy of NLCE, as well as additional numerical results, including a comparison of NLCE and matrix-product state simulations in the disordered 1D Heisenberg model.

[108] Note that for ladders, more complicated cluster shapes are in principle conceivable. In practice, it turns out that for such (quasi-)1D geometries, fully connected clusters yield a convincing convergence of the NLCE [99,101].

[109] K. Bhattaram and E. Khatami, Phys. Rev. E **100**, 013305 (2019).

[110] R. Schäfer, I. Hagymási, R. Moessner, and D. J. Luitz, Phys. Rev. B **102**, 054408 (2020).

[111] H. Tal-Ezer and R. Kosloff, J. Chem. Phys. **81**, 3967 (1984).

[112] V. V. Dobrovitski and H. De Raedt, Phys. Rev. E **67**, 056702 (2003).

[113] H. Fehske, J. Schleede, G. Schubert, G. Wellein, V. S. Filinov, and A. R. Bishop, Phys. Lett. A **373**, 2182 (2009).

[114] We calculate $\Delta \mathcal{I}$ as $\Delta \mathcal{I} = \frac{1}{\sqrt{N_s}} (\frac{1}{N_s} \sum_s [\mathcal{I}(t)]_s^2 - (\frac{1}{N_s} \sum_s [\mathcal{I}(t)]_s)^2)^{1/2}$, where $[\mathcal{I}(t)]_s$ denotes the imbalance $\mathcal{I}(t)$ for a single disorder realization and N_s is the number of disorder samples.

[115] Since $|\psi_2(0)\rangle$ is in the quarter-filling sector, which has a lower Hilbert-space dimension, the computational costs are reduced such that we consider slightly larger $c_{\max}$.

[116] V. Khemani, M. Hermele, and R. Nandkishore, Phys. Rev. B **101**, 174204 (2020).

[117] P. Sala, T. Rakovszky, R. Verresen, M. Knap, and F. Pollmann, Phys. Rev. X **10**, 011047 (2020).

[118] E. V. H. Doggen, I. V. Gornyi, and D. G. Polyakov, Phys. Rev. B **103**, L100202 (2021).

[119] M. Šroda, P. Prelovšek, and M. Mierzejewski, Phys. Rev. B **99**, 121110(R) (2019).

[120] V. K. Varma, A. Lerose, F. Pietracaprina, J. Goold, and A. Scardicchio, J. Stat. Mech. (2017) 053101.

[121] J. Richter, J. Herbrych, and R. Steinigeweg, Phys. Rev. B **98**, 134302 (2018).